

Article

# Cu-Mo<sub>2</sub>C/MCM-41: An Efficient Catalyst for the Selective Synthesis of Methanol from CO<sub>2</sub>

Xiaoran Liu, Yingquan Song, Wenhao Geng, Henan Li, Linfei Xiao and Wei Wu \*

International Joint Research Center of Catalytic Technology, Key Laboratory of Chemical Engineering Process & Technology for High-efficiency Conversion, College of Heilongjiang Province; School of Chemistry and Material Sciences, Heilongjiang University, Harbin 150080, China; liuxiaoranhljuh@tom.com (X.L.); songyingquanhljuh@tom.com (Y.S.); gengwenhaohljuh@tom.com (W.G.); lihenanhljuh@tom.com (H.L.); xiaolf@hlju.edu.cn (L.X.)

\* Correspondence: wuwe@hlju.edu.cn; Tel./Fax: +86-451-8660-9227

Academic Editor: Andreas Martin

Received: 26 April 2016; Accepted: 16 May 2016; Published: 20 May 2016

**Abstract:** Supported molybdenum carbide ( $\gamma$ -Mo<sub>2</sub>C/M41) and Cu-promoted molybdenum carbide, using a mechanical mixing and co-impregnation method ( $x$ Cu $\gamma$ Mo<sub>2</sub>C/M41-*M* and  $x$ Cu $\gamma$ Mo<sub>2</sub>C/M41-*I*) on a mesoporous molecular sieve MCM-41, were prepared by temperature-programmed carburization method in a CO/H<sub>2</sub> atmosphere at 1073 K, and their catalytic performances were tested for CO<sub>2</sub> hydrogenation to form methanol. Both catalysts, which were promoted by Cu, exhibited higher catalytic activity. In comparison to 20Cu20Mo<sub>2</sub>C/M41-*M*, the 20Cu20Mo<sub>2</sub>C/M41-*I* catalyst exhibited a stronger synergistic effect between Cu and Mo<sub>2</sub>C on the catalyst surface, which resulted in a higher selectivity for methanol in the CO<sub>2</sub> hydrogenation reaction. Under the optimal reaction conditions, the highest selectivity (63%) for methanol was obtained at a CO<sub>2</sub> conversion of 8.8% over the 20Cu20Mo<sub>2</sub>C/M41-*I* catalyst.

**Keywords:** CO<sub>2</sub> hydrogenation; Cu-promoted Mo<sub>2</sub>C; supported catalyst; methanol synthesis

## 1. Introduction

Due to increasing CO<sub>2</sub> emissions every year, human life and the environment have been greatly affected by global warming and climate changes [1,2]. The chemical utilization of CO<sub>2</sub>, which is the cheapest and most abundant C1 resource, has become an important global challenge [3–5]. Catalytic hydrogenation of CO<sub>2</sub> can produce various types of valuable chemicals and has been recently identified as one of the most promising processes for the utilization of CO<sub>2</sub> [6]. Among these processes, the synthesis of methanol from CO<sub>2</sub> is important because methanol can be used as a starting feedstock for chemical industries as well as an alternative to fossil fuels [7–10].

Over the past decades, significant efforts have been devoted to developing effective catalysts for CO<sub>2</sub> hydrogenation to form methanol. These studies primarily focused on modifying and improving the Cu/Zn-based catalyst by introducing suitable promoters or supports (e.g., Au [11], TiO<sub>2</sub> [12], Ga<sub>2</sub>O<sub>3</sub> [13,14], MgO [15], and CeO<sub>2</sub> [16]). In recent years, researchers found that the addition of an appropriate amount of ZrO<sub>2</sub> could enhance the copper dispersion and the surface basicity [17,18], and a high selectivity for methanol was obtained over the CuO/ZnO/ZrO<sub>2</sub> catalyst, while the conversion of CO<sub>2</sub> was limited [19]. In addition, some studies reported that the noble metal Pd could be used as an active component in catalysts for CO<sub>2</sub> hydrogenation to produce higher catalytic activity and methanol selectivity [20–22]. However, because both Cu/Zn-based and noble metal Pd catalysts have poor resistance to sulfur poisoning, their requirements for the purity of the feed gas are very high. Moreover, the wide industrial application of noble metal Pd catalyst is also limited due to its high cost.

Due to their unique tolerance of sulfur and potential alternatives to noble metals, transition metal carbides have attracted considerable attention in catalytic applications since the 1970s [23,24]. Molybdenum carbide exhibits catalytic properties similar to those of Pt or Pd catalysts, and this catalyst has been applied in various chemical reactions, such as the isomerization of *n*-heptane [25], steam reforming of methanol [26], dry reforming of methane [27], CO hydrogenation [28–30], and CO<sub>2</sub> hydrogenation [31–33]. Recently, researchers have demonstrated that a higher catalytic activity was obtained when another metal, which acted as a promoter, was introduced into the transition metal carbides, because the metal promoter results in the preferential formation of admetal-C bonds with significant electronic perturbations in the admetal [34]. Rodriguez *et al.* systematically studied the conversion of CO<sub>2</sub> into methanol catalyzed by  $\alpha$ -MoC<sub>1-x</sub>,  $\beta$ -Mo<sub>2</sub>C, Cu/ $\beta$ -Mo<sub>2</sub>C, Ni/ $\beta$ -Mo<sub>2</sub>C, and Co/ $\beta$ -Mo<sub>2</sub>C surfaces and found that Cu/ $\beta$ -Mo<sub>2</sub>C exhibited preferable catalytic activity for the selective synthesis of methanol [31,35]. Recently, they proposed a new route for methanol production over Cu/ $\beta$ -Mo<sub>2</sub>C catalysts by means of a combined experimental and theoretical study [36]. In this case, the Cu particles were effective sites for hydrogen dissociation and enhanced the hydrogen surface coverage [37]. However, the effects of the loading amount of Mo<sub>2</sub>C and Cu, as well as the degree of interaction between Cu and Mo<sub>2</sub>C on the catalytic performance for CO<sub>2</sub> hydrogenation, have not been previously investigated.

Usually, transition metal carbides are prepared using alkanes, alkene, and alkyne as carbon sources, but excess polymeric carbon from the pyrolysis of the carbonaceous gases at relatively low temperatures can deposit on the surface of the resultant carbide. To solve this problem, one strategy was to introduce H<sub>2</sub> into carburizing gas, which made it possible for deposited carbon species to be converted into gas hydrocarbon by hydrogenation [38,39]. In this study, a series of supported  $\gamma$ -Mo<sub>2</sub>C/M41 and Cu-promoted  $\gamma$ -Mo<sub>2</sub>C/M41 catalysts were prepared using the mixture of CO and H<sub>2</sub> as a carburizing gas, which can be derived from coal and heavy oil via steam reforming and applied to CO<sub>2</sub> hydrogenation to methanol. In particular, the effects of the degree of interaction between Cu and Mo<sub>2</sub>C on the surface of the catalysts, which were prepared using different methods, on the catalytic performance were investigated. In addition, the relationship between the catalytic performance and the surface property was studied.

## 2. Results and Discussion

### 2.1. Catalyst Characterization

#### 2.1.1. X-Ray Diffraction (XRD)

The XRD patterns of the  $\gamma$ -Mo<sub>2</sub>C/M41 samples with different Mo<sub>2</sub>C loadings are shown in Figure 1. Several peaks that were located at  $2\theta = 34.4^\circ, 38.0^\circ, 39.4^\circ, 52.1^\circ, 61.5^\circ, 69.5^\circ,$  and  $74.6^\circ$  were assigned to the  $\beta$ -Mo<sub>2</sub>C phase with a hexagonal closest packed (hcp) crystal structure, and the peak located at  $2\theta = 15^\circ$ – $30^\circ$  was attributed to the MCM-41 molecular sieve phase. However, for the 10Mo<sub>2</sub>C/M41 sample, the characteristic diffraction peaks corresponding to  $\beta$ -Mo<sub>2</sub>C were not observed, which may be due to the high dispersion of the Mo<sub>2</sub>C particles on the support. In addition, the intensity of the diffraction peaks corresponding to  $\beta$ -Mo<sub>2</sub>C became more intense as the Mo<sub>2</sub>C loading increased, which indicated that the crystallite size or crystallinity of  $\beta$ -Mo<sub>2</sub>C increased.

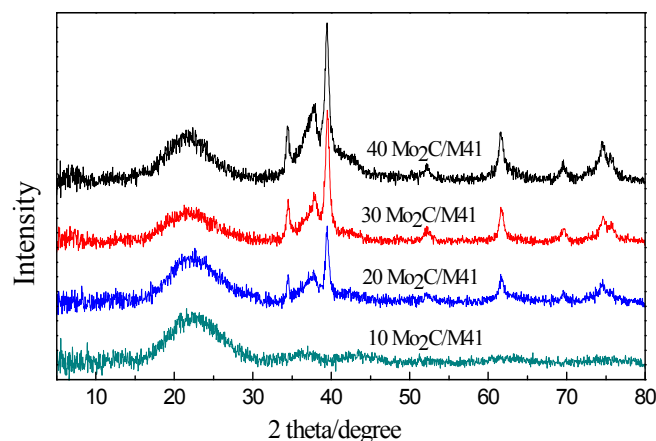


**Figure 1.** X-ray diffraction (XRD) patterns of the  $\gamma$ -Mo<sub>2</sub>C/M41 samples.

To improve the catalytic performance of 20Mo<sub>2</sub>C/M41, a series of  $x$ Cu20Mo<sub>2</sub>C/M41-*I* catalysts with different Cu loadings (12%, 20% and 28%) were prepared using the co-impregnation method, and the XRD patterns are shown in Figure 2. Except for several characteristic diffraction peaks corresponding to  $\beta$ -Mo<sub>2</sub>C phase, the peaks located at  $2\theta = 43.4^\circ$ ,  $50.5^\circ$ , and  $74.2^\circ$  were ascribed to Cu<sup>0</sup>. In addition, the peak located at  $2\theta = 36.7^\circ$  corresponded to  $\alpha$ -MoC<sub>1-x</sub>. These results indicated that the Cu promoter had a substantial effect on the crystal phase of molybdenum carbide [26,40]. As the Cu loading increased, the intensity of the diffraction peak corresponding to the Cu<sup>0</sup> phase increased (Figure 2), which indicated that the crystallite size of Cu<sup>0</sup> increased. This result is in agreement with the average crystallite size of Cu<sup>0</sup> in  $x$ Cu20Mo<sub>2</sub>C/M41-*I* (Table 1).

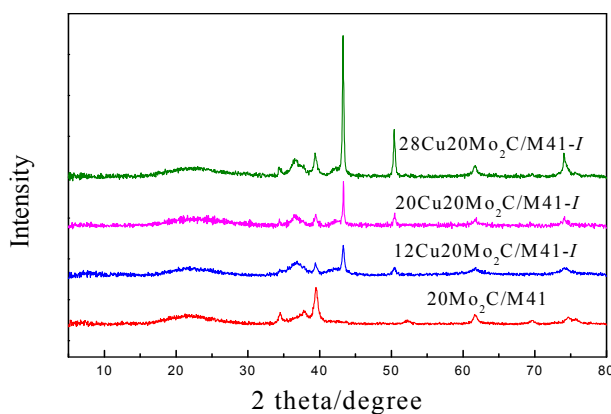


**Figure 2.** XRD patterns of the  $x$ Cu20Mo<sub>2</sub>C/M41-*I* samples.

**Table 1.** The average Cu crystallite size of the  $x$ Cu20Mo<sub>2</sub>C/M41-*I* samples.

Samples	Average Cu Crystallite Size (nm) <sup>1</sup>
12Cu20Mo <sub>2</sub> C/M41- <i>I</i>	10.2
20Cu20Mo <sub>2</sub> C/M41- <i>I</i>	24.4
28Cu20Mo <sub>2</sub> C/M41- <i>I</i>	33.5

<sup>1</sup> calculated by the Scherrer formula.

### 2.1.2. N<sub>2</sub> Adsorption–Desorption

The N<sub>2</sub> adsorption–desorption isotherms measured at 77.36 K allowed the textural properties of samples  $\gamma$ -Mo<sub>2</sub>C/M41 to be assessed, and the results are shown in Figure 3 and Table 2. All the samples

exhibited type IV isotherms as defined by the International Union of Pure and Applied Chemistry (IUPAC) classification with type H1 hysteresis loop at  $P/P_0 = 0.4-1.0$ . These results indicated that the mesoporous structure of MCM-41 was not destroyed when the catalysts were carbonized. However, the Brunauer-Emmett-Teller (BET) surface area and pore volume of the  $\gamma\text{Mo}_2\text{C}/\text{M41}$  samples decreased as the  $\text{Mo}_2\text{C}$  loading increased (Table 2), which suggests that a portion of the pores in MCM-41 was blocked by  $\text{Mo}_2\text{C}$ .

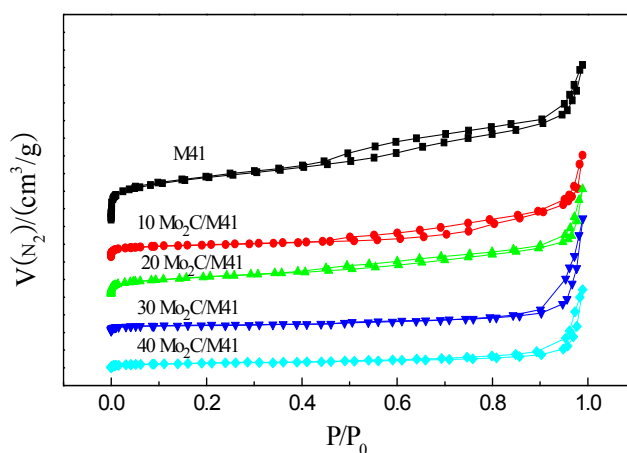


**Figure 3.**  $\text{N}_2$  adsorption and desorption isotherms of the  $\gamma\text{Mo}_2\text{C}/\text{M41}$  samples.

**Table 2.**  $\text{N}_2$  adsorption data of the  $\gamma\text{Mo}_2\text{C}/\text{M41}$  samples. BET: Brunauer-Emmett-Teller.

Samples	BET Surface Area ( $\text{m}^2/\text{g}$ )	Pore Volume ( $\text{cm}^3/\text{g}$ )
M41	1083	0.945
10 $\text{Mo}_2\text{C}/\text{M41}$	413	0.280
20 $\text{Mo}_2\text{C}/\text{M41}$	282	0.235
30 $\text{Mo}_2\text{C}/\text{M41}$	248	0.203
40 $\text{Mo}_2\text{C}/\text{M41}$	221	0.156

### 2.1.3. X-ray Photoelectron Spectroscopy (XPS)

The X-ray photoelectron spectroscopy (XPS) analysis was carried out to elucidate the surface properties of the catalysts. The Cu and Mo surface contents for  $x\text{Cu}20\text{Mo}_2\text{C}/\text{M41-I}$  are listed in Table 3. As shown in Table 3, as the Cu loading increased from 12% to 20%, the surface Cu atom content increased. When the Cu loading was 20%, the surface Cu atom content was the highest (*i.e.*, 43.8%). However, as the Cu loading continues to 28%, the surface Cu content decreased to 35.2% because Cu atoms agglomerated, leading to the formation of larger Cu particles that reduced the Cu content exposed on the surface of the catalyst. This result is consistent with the calculated average Cu crystallite size listed in Table 1.

**Table 3.** Surface Cu and Mo atom content of the  $x\text{Cu}20\text{Mo}_2\text{C}/\text{M41-I}$  samples.

Samples	Cu Atom Content (mol %)	Mo Atom Content (mol %)
12Cu20 $\text{Mo}_2\text{C}/\text{M41-I}$	35.7	64.3
20Cu20 $\text{Mo}_2\text{C}/\text{M41-I}$	43.8	56.2
28Cu20 $\text{Mo}_2\text{C}/\text{M41-I}$	35.2	64.8

In addition, the valence distribution of molybdenum on the catalyst surface was affected by the Cu loading. The Mo 3d XPS spectra of the 20 $\text{Mo}_2\text{C}/\text{M41}$  and  $x\text{Cu}20\text{Mo}_2\text{C}/\text{M41-I}$  samples are shown in Figure 4. As shown in Figure 4, the doublet peaks, which were assigned to Mo 3d<sub>5/2</sub> and

Mo  $3d_{3/2}$ , exhibited a splitting of  $\sim 3.13$  eV, and the ratio of Mo  $3d_{5/2}$  to Mo  $3d_{3/2}$  was 3:2. The XPS results suggested the presence of four molybdenum species as follows: the Mo  $3d_{5/2}$  binding energy of 228.8–229.0 eV corresponded to Mo<sup>II</sup> species involved in Mo–C bonding and the Mo  $3d_{5/2}$  binding energies of 229.6–229.8, 232.1–232.2, and 233.3–233.4 eV corresponded to Mo<sup>IV</sup> (MoO<sub>2</sub>), Mo <sup>$\delta$</sup>  (MoO<sub>x</sub>C<sub>y</sub>), and Mo<sup>VI</sup> (MoO<sub>3</sub>), respectively, in which the  $\delta$  was an intermediate oxidation state between 4 and 6 ( $4 < \delta < 6$ ) [26,41]. By curve fitting the Mo 3d profiles, the ratio of the surface Mo<sup>IV</sup> and Mo <sup>$\delta$</sup>  species to the total molybdenum species (*i.e.*, (Mo<sup>IV</sup> + Mo <sup>$\delta$</sup> )/Mo<sub>total</sub> (Mo<sub>total</sub> = Mo<sup>II</sup> + Mo<sup>IV</sup> + Mo <sup>$\delta$</sup>  + Mo<sup>VI</sup>)) was obtained and summarized in Table 4. When Cu was introduced to 20Mo<sub>2</sub>C/M41 using the co-impregnation method, the (Mo<sup>IV</sup> + Mo <sup>$\delta$</sup> )/Mo<sub>total</sub> ratio increased, and the ratio reached the highest value for the 20Cu20Mo<sub>2</sub>C/M41-I sample (Table 4). This result is similar to that reported by Liu where (Mo<sup>IV</sup> + Mo <sup>$\delta$</sup> )/Mo<sub>total</sub> increased when the Ca promoter was introduced into the Mo<sub>2</sub>C system [29].

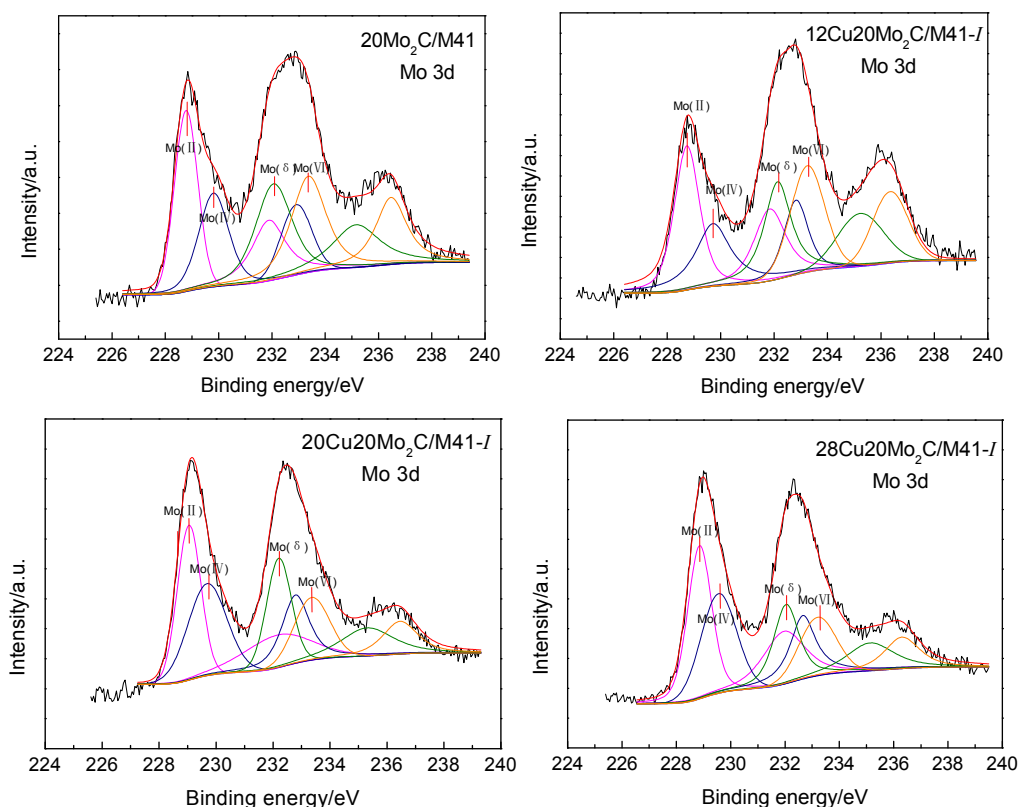


**Figure 4.** X-ray photoelectron spectroscopy (XPS) spectra of 20Mo<sub>2</sub>C/M41 and *x*Cu20Mo<sub>2</sub>C/M41-I.

**Table 4.** Mo  $3d_{5/2}$  binding energies and (Mo<sup>IV</sup> + Mo <sup>$\delta$</sup> )/Mo<sub>total</sub> ratios of 20Mo<sub>2</sub>C/M41 and *x*Cu20Mo<sub>2</sub>C/M41-I.

Samples	Mo $3d_{5/2}$ (eV)				(Mo <sup>IV</sup> + Mo <sup><math>\delta</math></sup> )/Mo <sub>total</sub> (%)
	Mo <sup>II</sup>	Mo <sup>IV</sup>	Mo <sup><math>\delta</math></sup>	Mo <sup>VI</sup>	
20Mo <sub>2</sub> C/M41	228.8	229.8	232.1	233.4	46.5
12Cu20Mo <sub>2</sub> C/M41-I	228.8	229.7	232.1	233.3	48.1
20Cu20Mo <sub>2</sub> C/M41-I	229.0	229.7	232.2	233.4	52.2
28Cu20Mo <sub>2</sub> C/M41-I	228.9	229.6	232.1	233.3	49.2

## 2.2. Catalytic Performance for the Hydrogenation of CO<sub>2</sub>

### 2.2.1. Catalytic Performance of the *y*Mo<sub>2</sub>C/M41 Samples

The catalytic performances of the *y*Mo<sub>2</sub>C/M41 samples were studied for the hydrogenation of CO<sub>2</sub> at 493 K under a pressure of 3.0 MPa and GHSV of 3600 mL/(h·g), and the results are shown in

Figure 5. The conversion of CO<sub>2</sub> increased from ~6% to ~8% as the Mo<sub>2</sub>C loading increased from 10% to 40%, which was due to a higher density of active sites on the catalyst surface. In this process, H<sub>2</sub> was activated by the forming C–H between the surface of Mo<sub>2</sub>C and the adsorbed H<sub>2</sub> [41]; at the same time, CO<sub>2</sub> was activated by the forming a C–C bond between the surface of Mo<sub>2</sub>C and the adsorbed CO<sub>2</sub> by a net carbide→CO<sub>2</sub> charge transfer [33]. As the Mo<sub>2</sub>C loading increased, a decrease in the selectivity of CH<sub>4</sub> was observed. However, the selectivity to CO increased. When the loading of Mo<sub>2</sub>C was 10% and 20%, the selectivity for CH<sub>3</sub>OH was higher, and a selectivity of 28% for CH<sub>3</sub>OH was observed over the 20Mo<sub>2</sub>C/M41 catalyst when the reaction was carried out for 14 h. However, the selectivity for CH<sub>3</sub>OH decreased when the Mo<sub>2</sub>C loading exceeded 30%, and more CO was produced. During the hydrogenation of CO<sub>2</sub>, CO and CH<sub>3</sub>OH were produced by two competitive pathways. The HOCO intermediate was formed firstly on the Mo<sub>2</sub>C surface. The cleavage of one C–O bond of the HOCO intermediate results in its decomposition to CO. However, the HOCO intermediate can transform into the HCOO intermediate, which can undergo stepwise hydrogenation to CH<sub>3</sub>OH [34,42]. Therefore, based on the effect of the Mo<sub>2</sub>C loading amount on CO<sub>2</sub> conversion and CH<sub>3</sub>OH selectivity, the optimal Mo<sub>2</sub>C loading was 20%.

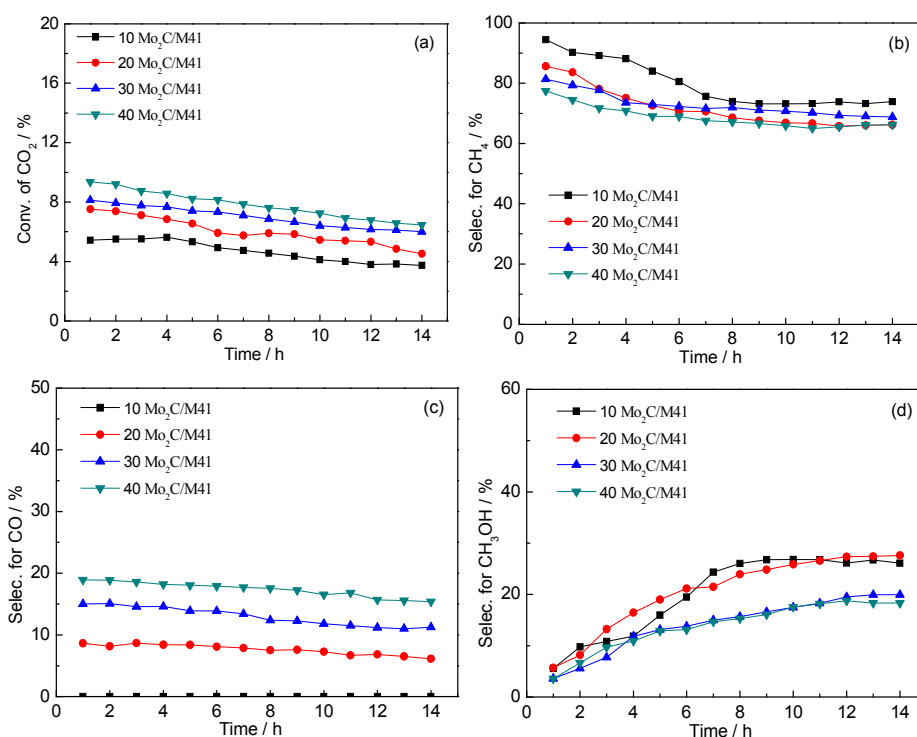


**Figure 5.** Catalytic performance of  $\gamma$ -Mo<sub>2</sub>C/M41 in CO<sub>2</sub> hydrogenation. (a) CO<sub>2</sub> conversion; (b) CH<sub>4</sub> selectivity; (c) CO selectivity; (d) CH<sub>3</sub>OH selectivity. Reaction conditions: catalyst 0.5 g, temperature 493 K, pressure 3.0 MPa (H<sub>2</sub>:CO<sub>2</sub> = 3:1), GHSV 3600 mL/(h·g).

### 2.2.2. Catalytic Performance for the Cu-Promoted 20Mo<sub>2</sub>C/M41 Catalyst

Due to the high capability of the Cu promoter to absorb and activate H<sub>2</sub> [37], which are beneficial to CO<sub>2</sub> hydrogenation, a series of Cu-promoted 20Mo<sub>2</sub>C/M41 catalysts were prepared using the mechanical mixing method (*M*) and the co-impregnation method (*I*) (*i.e.* 20Cu20Mo<sub>2</sub>C/M41-*M* and 20Cu20Mo<sub>2</sub>C/M41-*I*, respectively), and their catalytic performances were evaluated for CO<sub>2</sub> hydrogenation to synthesize CH<sub>3</sub>OH. As shown in Figure 6, both 20Cu/M41 and 20Mo<sub>2</sub>C/M41 catalysts exhibited low CO<sub>2</sub> conversion and methanol selectivity. However, the CO<sub>2</sub> conversion and CH<sub>3</sub>OH selectivity increased over the 20Cu20Mo<sub>2</sub>C/M41-*M* catalyst (mechanical mixing 20Cu/M41 and 20Mo<sub>2</sub>C/M41). When 20Cu20Mo<sub>2</sub>C/M41-*I* prepared by co-impregnation method was employed

as the catalyst, its catalytic performance further improved. Furthermore, regardless of the method used to introduce the Cu promoter to 20Mo<sub>2</sub>C/M41 catalytic system, the CO<sub>2</sub> conversion and CH<sub>3</sub>OH selectivity increased, and the selectivity to CH<sub>4</sub> and CO decreased. This indicated that there was a synergetic effect between Cu and Mo<sub>2</sub>C in the hydrogenation of CO<sub>2</sub> when the Cu-promoted supported molybdenum carbide was used as a catalyst. In the hydrogenation of CO<sub>2</sub>, the adsorption and activation of hydrogen primarily occurred on Cu sites; in addition, the adsorption and activation of CO<sub>2</sub> occurred over Mo<sub>2</sub>C sites in the Cu–Mo<sub>2</sub>C/M41 system (Scheme 1). In particular, the CO<sub>2</sub> molecule was attached to the Mo<sub>2</sub>C surface, and a C–C bond was formed between the surface and the adsorbate by a net carbide→CO<sub>2</sub> charge transfer. Simultaneously, some bonding interactions were generated between the O atoms of CO<sub>2</sub> and nearby Mo atoms [33]. Then, the activated hydrogen was transported from the Cu surface to the Mo<sub>2</sub>C surface sites via spillover followed by hydrogenation of the adsorbed CO<sub>2</sub> to form the HOCO intermediate. The HOCO intermediate decomposed to CO due to cleavage of the C–O bond. If the C–O bond of CO cracked continually, C was produced, which was hydrogenated to yield CH<sub>4</sub>. However, the HOCO intermediate was isomerized to the HCOO intermediate, which underwent stepwise hydrogenation to CH<sub>3</sub>OH [34,42]. In combination with the experimental results shown in Figure 6, the introduction of Cu in 20Cu20Mo<sub>2</sub>C/M41 increased the concentration of Mo<sup>IV</sup> and Mo<sup>δ</sup> cations, which may be favorable for the isomerization of HOCO to HCOO, leading to an increase in the CH<sub>3</sub>OH selectivity.

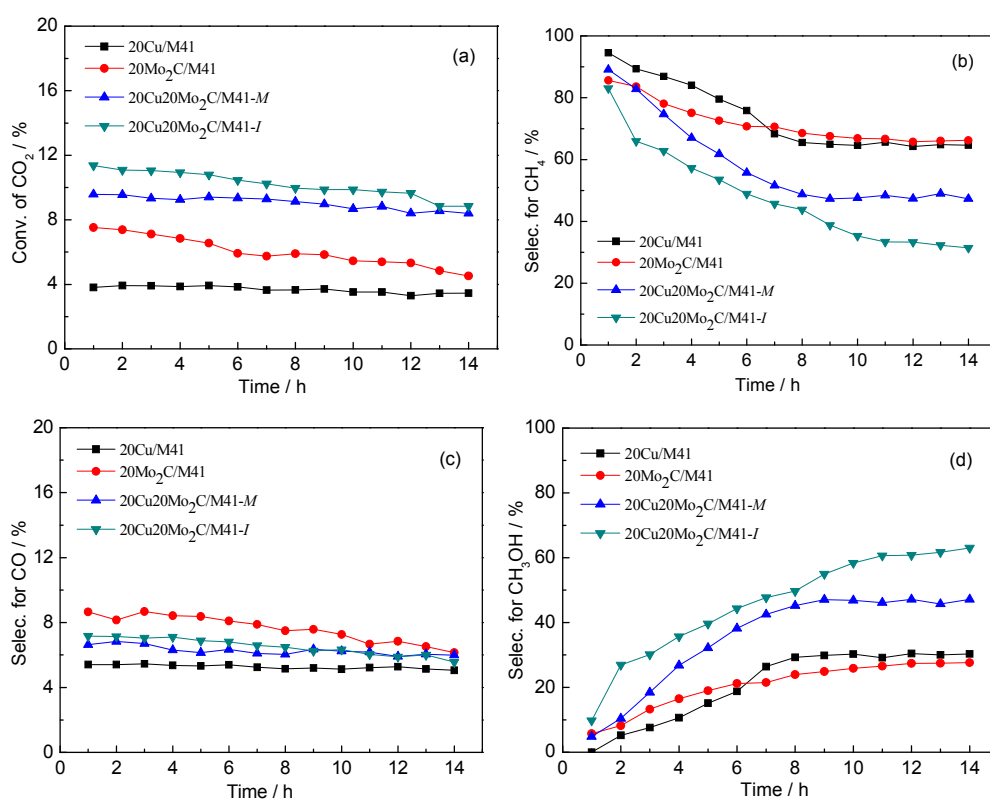
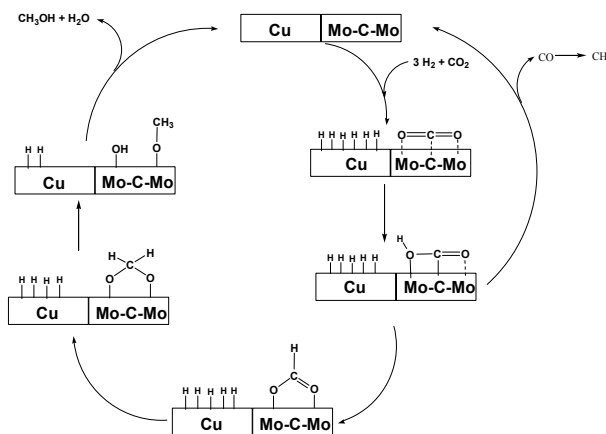


**Figure 6.** Catalytic performance of 20Cu20Mo<sub>2</sub>C/M41 with different introducing method of Cu promoter in CO<sub>2</sub> hydrogenation. (a) CO<sub>2</sub> conversion; (b) CH<sub>4</sub> selectivity; (c) CO selectivity; (d) CH<sub>3</sub>OH selectivity. Reaction conditions: catalyst 0.5 g, temperature 493 K, pressure 3.0 MPa (H<sub>2</sub>:CO<sub>2</sub> = 3:1), GHSV 3600 mL/(h·g).



**Scheme 1.** Proposed reaction mechanism for CO<sub>2</sub> hydrogenation over Cu–Mo<sub>2</sub>C/M41 catalysts.

In comparison to 20Cu20Mo<sub>2</sub>C/M41-*M*, the 20Cu20Mo<sub>2</sub>C/M41-*I* catalyst exhibited a higher CO<sub>2</sub> conversion and CH<sub>3</sub>OH selectivity because the Cu particles were highly dispersed on the support in 20Cu20Mo<sub>2</sub>C/M41-*I*, which enhanced the interaction between Cu and Mo<sub>2</sub>C. In addition, H<sub>2</sub> can be easily adsorbed and activated on Cu atoms, with the dissociated H spillover followed by the Mo<sub>2</sub>C surface, to add to a H reservoir that is available for the sequential hydrogenation of CO<sub>2</sub> at the Mo-carbide interface, which led to an improvement in the catalytic performance of 20Cu20Mo<sub>2</sub>C/M41-*I* in the hydrogenation of CO<sub>2</sub>. In particular, the CH<sub>3</sub>OH selectivity significantly increased, which is consistent with previously reported results [43].

These results indicate that a higher CH<sub>3</sub>OH selectivity can be achieved when the co-impregnation method was used to introduce Cu into the 20Mo<sub>2</sub>C/M41 catalytic system. Therefore, the effects of Cu loading on the catalytic performance of the *x*Cu20Mo<sub>2</sub>C/M41-*I* catalysts in CO<sub>2</sub> hydrogenation were also studied, and the results are shown in Figure 7. When the Cu loading increased to 20%, the highest content of Cu was observed on the catalyst surface (Table 3), and the loaded Cu was beneficial for the activation of H<sub>2</sub> and had a substantial positive effect on the conversion of CO<sub>2</sub>. The highest CO<sub>2</sub> conversion was 11.4%; however, the conversion of CO<sub>2</sub> decreased when the Cu loading was 28% because the size of the Cu particles increased. In addition, the Cu atom content exposed on the surface of the catalyst decreased (Tables 1 and 3). When Cu was introduced to the catalyst system as a promoter, the selectivity of the catalysts for CH<sub>4</sub> and CO decreased, and the CH<sub>3</sub>OH selectivity increased. This result may be due to the promotion of the isomerization of HOCO to HCOO when 20Mo<sub>2</sub>C/M41 was modified by Cu. The highest selectivity (63%) for methanol was obtained at a CO<sub>2</sub> conversion of 8.8% over the 20Cu20Mo<sub>2</sub>C/M41-*I* catalyst because the highest amount of Mo<sup>IV</sup> and Mo<sup>δ</sup> species was detected on the catalyst surface, which favored the synthesis of methanol. The same results were found in the literature [29].

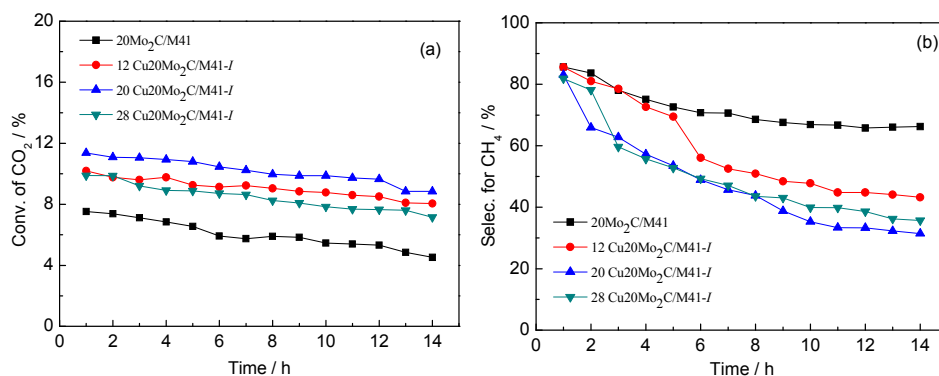


**Figure 7.** Cont.

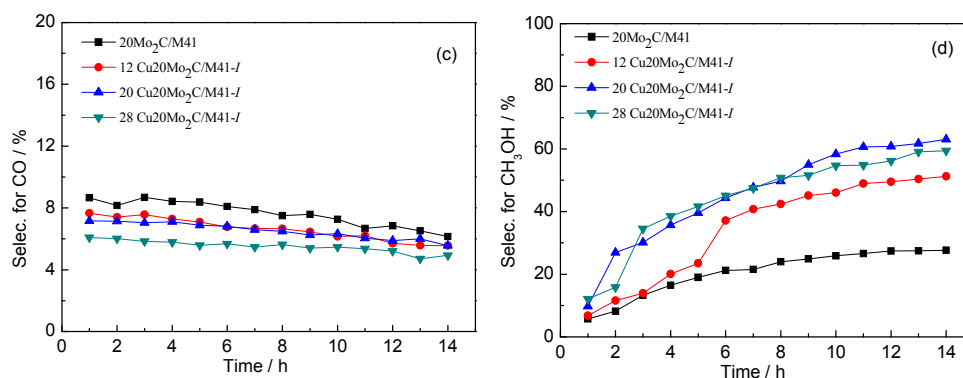


**Figure 7.** Catalytic performance of  $x\text{Cu}20\text{Mo}_2\text{C}/\text{M41-I}$  in  $\text{CO}_2$  hydrogenation. (a)  $\text{CO}_2$  conversion; (b)  $\text{CH}_4$  selectivity; (c)  $\text{CO}$  selectivity; (d)  $\text{CH}_3\text{OH}$  selectivity. Reaction conditions: catalyst 0.5 g, temperature 493 K, pressure 3.0 MPa ( $\text{H}_2:\text{CO}_2 = 3:1$ ), GHSV 3600 mL/(h·g).

### 2.2.3. The Stability of the $20\text{Cu}20\text{Mo}_2\text{C}/\text{M41-I}$ Catalyst

In order to study the stability of the  $20\text{Cu}20\text{Mo}_2\text{C}/\text{M41-I}$  catalyst, we investigated its catalytic performance over 110 h, and the results are presented in Figure 8. It can be seen that the stable catalytic performance was given when the  $20\text{Cu}20\text{Mo}_2\text{C}/\text{M41-I}$  catalyst was used for more than 10 h. When the reaction was carried out for 110 h, the selectivity for methanol and the conversion of  $\text{CO}_2$  remained stable, which exhibited an excellent stability in  $\text{CO}_2$  hydrogenation.

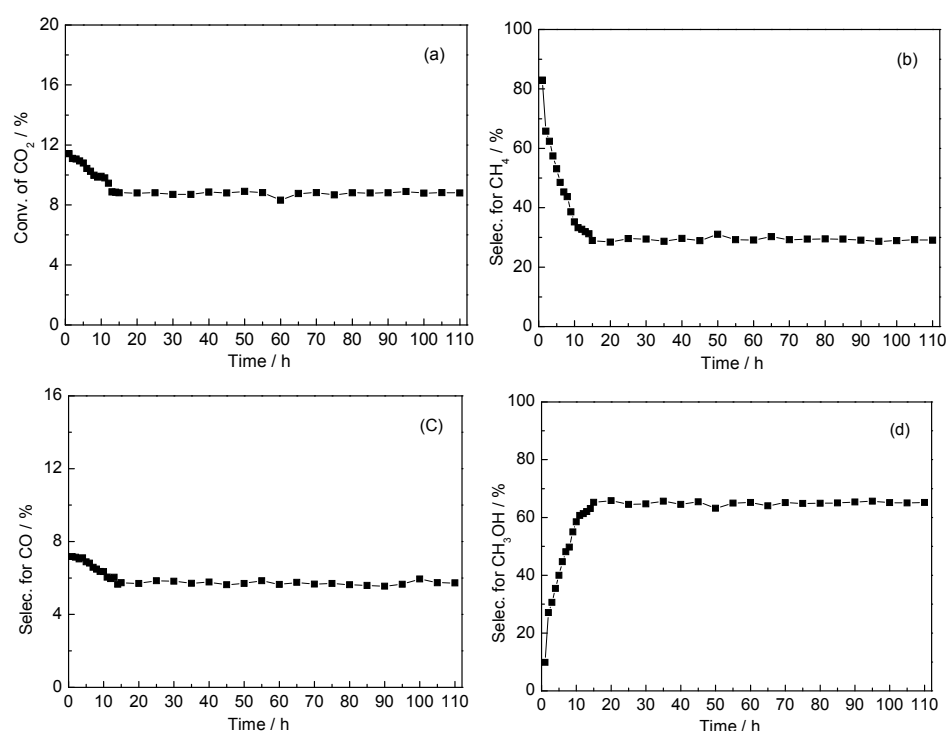


**Figure 8.** Catalytic performance of  $20\text{Cu}20\text{Mo}_2\text{C}/\text{M41-I}$  in  $\text{CO}_2$  hydrogenation. (a)  $\text{CO}_2$  conversion; (b)  $\text{CH}_4$  selectivity; (c)  $\text{CO}$  selectivity; (d)  $\text{CH}_3\text{OH}$  selectivity. Reaction conditions: catalyst 0.5 g, temperature 493 K, pressure 3.0 MPa ( $\text{H}_2:\text{CO}_2 = 3:1$ ), GHSV 3600 mL/(h·g).

### 3. Experimental Section

#### 3.1. Catalyst Preparation

The catalysts were prepared by incipient wetness co-impregnation onto MCM-41 (purchased from Nankai University Catalyst Co., Ltd. Tianjin, China) with an aqueous solution consisting of  $(\text{NH}_4)_6\text{Mo}_7\text{O}_{24} \cdot 4\text{H}_2\text{O}$  and  $\text{Cu}(\text{NO}_3)_2 \cdot 3\text{H}_2\text{O}$ . Then, the catalysts were dried overnight at 373 K, followed by calcination at 923 K for 3 h to afford supported molybdenum oxide and copper oxide. Carburization of the catalysts was accomplished using a temperature-programmed reaction. Specifically, this step was performed in a quartz tube reactor by heating at a rate of  $10 \text{ K} \cdot \text{min}^{-1}$  from room temperature to 573 K and then at a rate of  $1 \text{ K} \cdot \text{min}^{-1}$  from 573 to 1073 K in 20%  $\text{CO}/\text{H}_2$  mixture, and the temperature was maintained at 1073 K for 4 h. The catalysts were subsequently cooled to room temperature in  $\text{H}_2$ , followed by passivation in a stream of 1%  $\text{O}_2/\text{N}_2$  mixture at room temperature for 2 h prior to exposure to air. These catalysts are referred to as  $x\text{Cu}y\text{Mo}_2\text{C}/\text{M41-}I$ , where  $x$  and  $y$  represent the mass percentages of Cu and  $\text{Mo}_2\text{C}$ , respectively, and  $I$  refers to the co-impregnation method. In addition,  $x\text{Cu}y\text{Mo}_2\text{C}/\text{M41-}M$  was prepared by mechanical mixing and grinding  $x\text{Cu}/\text{M41}$  and  $y\text{Mo}_2\text{C}/\text{M41}$ , where  $M$  refers to the mechanical mixing method.

#### 3.2. Characterization

Powder XRD patterns of the prepared samples were recorded on a Bruker D8 Advance diffractometer using  $\text{Cu K}\alpha$  ( $\lambda = 1.5404 \text{ \AA}$ ) irradiation at 40 kV and 40 mA with a Lynx eye detector in the range of  $2\theta = 5^\circ\text{--}80^\circ$ . The  $\text{N}_2$  adsorption–desorption characterization of the samples was performed using an Autosorb-1-MP apparatus (Quantachrome Instruments, Boynton Beach, FL, USA). Prior to the adsorption measurements, the catalysts were degassed under vacuum for nearly 12 h at 573 K. The specific surface areas were calculated using the Brunauer-Emmett-Teller (BET) method. The pore volumes were estimated from the desorption branch of the  $\text{N}_2$  adsorption-desorption isotherms by applying the Barrett-Joyner-Halenda (BJH) method. The XPS analyses were performed using a Surface Science Instruments spectrometer (ESCALAB 250) (Waltham, MA, USA) with focused  $\text{Al K}\alpha$  radiation (1486.6 eV).

#### 3.3. Catalytic Test

The performances of the catalysts for  $\text{CO}_2$  hydrogenation were investigated under pressurized conditions with a high-pressure fixed bed reactor system. A 0.5-g portion of the catalyst was placed in the reactor along with inert quartz sands above and below the catalyst. All the catalysts were reduced in a flow of hydrogen at 673 K for 1 h prior to the reaction. When the temperature was cooled from 673 K to 493 K, the feed gas (*i.e.*,  $\text{CO}_2/\text{H}_2/\text{Ar}$  ( $\text{H}_2:\text{CO}_2$  volume ratio was 3:1)) flowed into the system at a pressure of 3.0 MPa and GHSV of 3600  $\text{mL}/(\text{h} \cdot \text{g})$ . All the products were produced in the gaseous state and analyzed using a gas chromatograph (GC). Ar, CO and  $\text{CO}_2$  were analyzed using a GC equipped with a thermal conductivity detector (TCD) and a column consisting of activated charcoal.  $\text{CH}_4$  and  $\text{CH}_3\text{OH}$  were analyzed using another GC equipped with a flame ionization detector (FID). Ar was used as the internal standard for the GC/TCD analyses. It was important to note that only trace amounts of  $\text{C}_2\text{H}_6$ ,  $\text{C}_3\text{H}_8$ , and  $\text{CH}_3\text{OCH}_3$  were detected in the products, and their content was ignored.

### 4. Conclusions

In summary, the catalytic performance of  $y\text{Mo}_2\text{C}/\text{M41}$  for the hydrogenation of  $\text{CO}_2$  to methanol can be tuned by loading the appropriate amount of  $\text{Mo}_2\text{C}$ . Among these catalysts, the  $20\text{Mo}_2\text{C}/\text{M41}$  catalyst exhibited excellent catalytic performance. When Cu was introduced to  $20\text{Mo}_2\text{C}/\text{M41}$  by the mechanical mixing method ( $M$ ) and co-impregnation method ( $I$ ), the catalytic performance improved to different extents. In the  $\text{Cu-Mo}_2\text{C}/\text{M41}$  catalytic system, a synergistic effect was observed between Cu and  $\text{Mo}_2\text{C}$  on the catalyst surface. Therefore, the adsorption and activation of hydrogen primarily occurred on Cu sites, and the adsorption of  $\text{CO}_2$  occurred over  $\text{Mo}_2\text{C}$  sites.

In addition, the introduction of Cu increased the concentration of Mo<sup>IV</sup> and Mo<sup>δ</sup> cations, which may be beneficial to the isomerization of HOCO to HCOO, leading to an increase in CH<sub>3</sub>OH selectivity. In comparison to 20Cu20Mo<sub>2</sub>C/M41-M, the 20Cu20Mo<sub>2</sub>C/M41-I catalyst exhibited significantly increased CH<sub>3</sub>OH selectivity because the Cu promoter was highly dispersed on the surface of the catalyst. In addition, enhanced interactions existed between Cu and Mo<sub>2</sub>C active sites. The valence distribution of molybdenum on the catalyst surface was affected by loaded Cu introduced by the co-impregnation method. When the Cu loading amount was 20%, the surface Cu atom content was the highest with the largest amount of Mo<sup>IV</sup> and Mo<sup>δ</sup> species, and the highest selectivity (63%) for methanol was obtained at a CO<sub>2</sub> conversion of 8.8% and excellent stability during 110 h was observed over it.

**Acknowledgments:** This work was supported by Programs of International S&T cooperation (2013DFR40570, 2014DFR41110).

**Author Contributions:** Xiaoran Liu, Yingquan Song, Wenhao Geng, and Henan Li performed the experiment. Wei Wu and Linfei Xiao analyzed and discussed the experimental results. Xiaoran Liu wrote the paper.

**Conflicts of Interest:** The authors declare no conflict of interest.

## References

1. Aresta, M.; Dibenedetto, A.; Angelini, A. Catalysis for the valorization of exhaust carbon: From CO<sub>2</sub> to chemicals, materials, and fuels. Technological use of CO<sub>2</sub>. *Chem. Rev.* **2014**, *114*, 1709–1742. [[CrossRef](#)] [[PubMed](#)]
2. Du, X.L.; Jiang, Z.; Su, D.S.; Wang, J.Q. Research progress on the indirect hydrogenation of carbon dioxide to methanol. *ChemSusChem* **2016**, *9*, 322–332. [[CrossRef](#)] [[PubMed](#)]
3. Ganesh, I. Conversion of carbon dioxide into methanol—a potential liquid fuel: Fundamental challenges and opportunities. *Renew. Sust. Energy Rev.* **2014**, *31*, 221–257. [[CrossRef](#)]
4. Wang, W.H.; Himeda, Y.; Muckerman, J.T.; Manbeck, G.F.; Fujita, E. CO<sub>2</sub> hydrogenation to formate and methanol as an alternative to photo- and electrochemical CO<sub>2</sub> reduction. *Chem. Rev.* **2015**, *115*, 12936–12973. [[CrossRef](#)] [[PubMed](#)]
5. Ali, K.A.; Abdullah, A.Z.; Mohamed, A.R. Recent development in catalytic technologies for methanol synthesis from renewable sources: A critical review. *Renew. Sust. Energy Rev.* **2015**, *44*, 508–518. [[CrossRef](#)]
6. Liang, X.L.; Xie, J.R.; Liu, Z.M. A novel Pd-decorated carbon nanotubes-promoted Pd-ZnO catalyst for CO<sub>2</sub> hydrogenation to methanol. *Catal. Lett.* **2015**, *145*, 1138–1147. [[CrossRef](#)]
7. Kong, H.; Li, H.Y.; Lin, G.D.; Zhang, H.B. Pd-decorated CNT-promoted Pd-Ga<sub>2</sub>O<sub>3</sub> catalyst for hydrogenation of CO<sub>2</sub> to methanol. *Catal. Lett.* **2011**, *141*, 886–894. [[CrossRef](#)]
8. Koizumi, N.; Jiang, X.; Kugai, J.; Song, C.S. Effects of mesoporous silica supports and alkaline promoters on activity of Pd catalysts in CO<sub>2</sub> hydrogenation for methanol synthesis. *Catal. Today* **2012**, *194*, 16–24. [[CrossRef](#)]
9. Jiang, X.; Koizumi, N.; Guo, X.W.; Song, C.S. Bimetallic Pd-Cu catalysts for selective CO<sub>2</sub> hydrogenation to methanol. *Appl. Catal. B-Environ.* **2015**, *170–171*, 173–185. [[CrossRef](#)]
10. Olah, G.A. After oil and gas: Methanol economy. *Catal. Lett.* **2004**, *93*, 1–2. [[CrossRef](#)]
11. Pasupulety, N.; Driss, H.; Alhamed, Y.A.; Alzahrani, A.A.; Daous, M.A.; Petrov, L. Studies on Au/Cu-Zn-Al catalyst for methanol synthesis from CO<sub>2</sub>. *Appl. Catal. A-Gen.* **2015**, *504*, 308–318. [[CrossRef](#)]
12. Graciani, J.; Mudiyansele, K.; Xu, F.; Baber, A.E.; Evans, J.; Senanayake, S.D.; Stacchiola, D.J.; Liu, P.; Hrbek, J.; Sanz, J.F. Highly active copper-ceria and copper-ceria-titania catalysts for methanol synthesis from CO<sub>2</sub>. *Science* **2014**, *345*, 546–550. [[CrossRef](#)] [[PubMed](#)]
13. Ladera, R.; Pérez-Alonso, F.J.; González-Carballo, J.M.; Ojeda, M.; Rojas, S.; Fierro, J.L.G. Catalytic valorization of CO<sub>2</sub> via methanol synthesis with Ga-promoted Cu-ZnO-ZrO<sub>2</sub> catalysts. *Appl. Catal. B-Environ.* **2013**, *142–143*, 241–248. [[CrossRef](#)]
14. Toyir, J.; de la Piscina, P.R.; Homs, N. Ga-promoted copper-based catalysts highly selective for methanol steam reforming to hydrogen; relation with the hydrogenation of CO<sub>2</sub> to methanol. *Int. J. Hydrogen. Energy* **2015**, *40*, 11261–11266. [[CrossRef](#)]

15. Ren, H.; Xu, C.H.; Zhao, H.Y.; Wang, Y.X.; Liu, J.; Liu, J.Y. Methanol synthesis from CO<sub>2</sub> hydrogenation over Cu/ $\gamma$ -Al<sub>2</sub>O<sub>3</sub> catalysts modified by ZnO, ZrO<sub>2</sub> and MgO. *J. Ind. Eng. Chem.* **2015**, *28*, 261–267. [[CrossRef](#)]
16. Senanayake, S.D.; Ramírez, P.J.; Waluyo, I.; Kundu, S.; Mudiyansele, K.; Liu, Z.Y.; Liu, Z.; Axnanda, S.; Stacchiola, D.J.; Evans, J.; *et al.* Hydrogenation of CO<sub>2</sub> to methanol on CeO<sub>x</sub>/Cu(111) and ZnO/Cu(111) catalysts: Role of the metal-oxide interface and importance of Ce<sup>3+</sup> sites. *J. Phys. Chem. C* **2016**, *120*, 1778–1784. [[CrossRef](#)]
17. Huang, C.J.; Chen, S.Y.; Fei, X.Y.; Liu, D.; Zhang, Y.C. Catalytic hydrogenation of CO<sub>2</sub> to methanol: Study of synergistic effect on adsorption properties of CO<sub>2</sub> and H<sub>2</sub> in CuO/ZnO/ZrO<sub>2</sub> system. *Catalysts* **2015**, *5*, 1846–1861. [[CrossRef](#)]
18. Gao, P.; Li, F.; Zhan, H.J.; Zhao, N.; Xiao, F.K.; Wei, W.; Zhong, L.S.; Wang, H.; Sun, Y.H. Influence of Zr on the performance of Cu/Zn/Al/Zr catalysts via hydrotalcite-like precursors for CO<sub>2</sub> hydrogenation to methanol. *J. Catal.* **2013**, *298*, 51–60. [[CrossRef](#)]
19. Arena, F.; Mezzatesta, G.; Zafarana, G.; Trunfio, G.; Frusteri, F.; Spadaro, L. Effects of oxide carriers on surface functionality and process performance of the Cu-ZnO system in the synthesis of methanol via CO<sub>2</sub> hydrogenation. *J. Catal.* **2013**, *300*, 141–151. [[CrossRef](#)]
20. Collins, S.E.; Delgado, J.J.; Mira, C.; Calvino, J.J.; Bernal, S.; Chiavassa, D.L.; Baltanás, M.A.; Bonivardi, A.L. The role of Pd-Ga bimetallic particles in the bifunctional mechanism of selective methanol synthesis via CO<sub>2</sub> hydrogenation on a Pd/Ga<sub>2</sub>O<sub>3</sub> catalyst. *J. Catal.* **2012**, *292*, 90–98. [[CrossRef](#)]
21. Song, Y.Q.; Liu, X.R.; Xiao, L.F.; Wu, W.; Zhang, J.W.; Song, X.M. Pd-Promoter/MCM-41: A highly effective bifunctional catalyst for conversion of carbon dioxide. *Catal. Lett.* **2015**, *145*, 1272–1280. [[CrossRef](#)]
22. Chiavassa, D.L.; Barrandeguy, J.; Bonivardi, A.L.; Baltanas, M.A. Methanol synthesis from CO<sub>2</sub>/H<sub>2</sub> using Ga<sub>2</sub>O<sub>3</sub>-Pd/silica catalysts: Impact of reaction products. *Catal. Today* **2008**, *133–135*, 780–786. [[CrossRef](#)]
23. Dhandapani, B.; Ramanathan, S.; Yu, C.C.; Frühberger, B.; Chen, J.G.; Oyama, S.T. Synthesis, characterization, and reactivity studies of supported Mo<sub>2</sub>C with phosphorus additive. *J. Catal.* **1998**, *176*, 61–67. [[CrossRef](#)]
24. Levy, R.B.; Boudart, M. Platinum-like behavior of tungsten carbide in surface catalysis. *Science* **1973**, *181*, 547–579. [[CrossRef](#)] [[PubMed](#)]
25. Lamic, A.F.; Pham, T.L.H.; Potvin, C.; Manoli, J.M.; Mariadassou, G.D. Kinetics of bifunctional isomerization over carbides (Mo, W). *J. Mol. Catal. A-Chem.* **2005**, *237*, 109–114. [[CrossRef](#)]
26. Ma, Y.F.; Guan, G.Q.; Hao, X.G.; Zuo, Z.J.; Huang, W.; Phanthong, P.; Kusakabe, K.; Abudula, A. Highly-efficient steam reforming of methanol over copper modified molybdenum carbide. *RSC. Adv.* **2014**, *4*, 44175–44184. [[CrossRef](#)]
27. Shi, C.; Zhang, A.J.; Li, X.S.; Zhang, S.H.; Zhu, A.M.; Ma, Y.F. Ni-modified Mo<sub>2</sub>C catalysts for methane dry reforming. *Appl. Catal. A-Gen.* **2012**, *431–432*, 164–170. [[CrossRef](#)]
28. Christensen, J.M.; Duchstein, L.D.L.; Wagner, J.B.; Jensen, P.A.; Temel, B.; Jensen, A.D. Catalytic conversion of syngas into higher alcohols over carbide catalysts. *Ind. Eng. Chem. Res.* **2012**, *51*, 4161–4172. [[CrossRef](#)]
29. Liu, C.C.; Lin, M.G.; Jiang, D.; Fang, K.G.; Sun, Y.H. Preparation of promoted molybdenum carbides nanowire for CO hydrogenation. *Catal. Lett.* **2014**, *144*, 567–573. [[CrossRef](#)]
30. Yin, K.H.; Shou, H.; Ferrari, D.; Jones, C.W.; Davi, R.J. Influence of cobalt on rubidium-promoted alumina-supported molybdenum carbide catalysts for higher alcohol synthesis from syngas. *Top. Catal.* **2013**, *56*, 1740–1751. [[CrossRef](#)]
31. Xu, W.Q.; Ramirez, P.J.; Stacchiola, D.; Rodriguez, J.A. Synthesis of  $\alpha$ -MoC<sub>1-x</sub> and  $\beta$ -MoC<sub>y</sub> catalysts for CO<sub>2</sub> hydrogenation by thermal carburization of Mo-oxide in hydrocarbon and hydrogen mixtures. *Catal. Lett.* **2014**, *144*, 1418–1424. [[CrossRef](#)]
32. Nagai, M.; Oshikawa, K.; Kurakami, T.; Miyao, T.; Omi, S. Surface properties of carbided molybdena-alumina and its activity for CO<sub>2</sub> hydrogenation. *J. Catal.* **1998**, *180*, 14–23. [[CrossRef](#)]
33. Posada-Pérez, S.; Viñes, F.; Ramirez, J.A.; Vidal, A.B.; Rodriguez, J.A.; Illas, F. The bending machine: CO<sub>2</sub> activation and hydrogenation on  $\delta$ -MoC(001) and  $\beta$ -Mo<sub>2</sub>C(001) surfaces. *Phys. Chem. Chem. Phys.* **2014**, *16*, 14912–14921. [[CrossRef](#)] [[PubMed](#)]
34. Rodriguez, J.A.; Evans, J.; Feria, L.; Vidal, A.B.; Liu, P.; Nakamura, K.; Illas, F. CO<sub>2</sub> hydrogenation on Au/TiC, Cu/TiC, and Ni/TiC catalysts: Production of CO, methanol, and methane. *J. Catal.* **2013**, *307*, 162–169. [[CrossRef](#)]

35. Xu, W.Q.; Ramírez, P.J.; Stacchiola, D.; Brito, J.L.; Rodriguez, J.A. The carburization of transition metal molybdates ( $M_xMoO_4$ ,  $M=Cu, Ni$  or  $Co$ ) and the generation of highly active metal/carbide catalysts for  $CO_2$  hydrogenation. *Catal. Lett.* **2015**, *145*, 1365–1373. [[CrossRef](#)]
36. Posada-Pérez, S.; Ramírez, P.J.; Gutiérrez, R.A.; Stacchiola, D.J.; Viñes, F.; Liu, P.; Illas, F.; Rodriguez, J.A. The conversion of  $CO_2$  to methanol on orthorhombic  $\beta-Mo_2C$  and  $Cu/\beta-Mo_2C$  catalysts: Mechanism for admetal induced change in the selectivity and activity. *Catal. Sci. Technol.* **2016**. [[CrossRef](#)]
37. Chen, Y.; Choi, S.; Thompson, L.T. Low-temperature  $CO_2$  hydrogenation to liquid products via a heterogeneous cascade catalytic system. *ACS Catal.* **2015**, *5*, 1717–1725. [[CrossRef](#)]
38. Wang, X.H.; Hao, H.L.; Zhang, M.H.; Li, W.; Tao, K.Y. Synthesis and characterization of molybdenum carbides using propane as carbon source. *J. Solid State Chem.* **2006**, *179*, 538–543. [[CrossRef](#)]
39. Xiao, T.; York, A.P.E.; Williams, V.C.; Al-Megren, H.; Hanif, A.; Zhou, X.; Green, M.L.H. Preparation of molybdenum carbides using butane and their catalytic performance. *Chem. Mater.* **2000**, *12*, 3896–3905. [[CrossRef](#)]
40. Jung, K.T.; Kim, W.B.; Rhee, C.H.; Lee, J.S. Effects of transition metal addition on the solid-state transformation of molybdenum trioxide to molybdenum carbides. *Chem. Mater.* **2004**, *16*, 307–314. [[CrossRef](#)]
41. Liu, C.C.; Lin, M.G.; Fang, K.G.; Meng, Y.; Sun, Y.H. Preparation of nanostructured molybdenum carbides for CO hydrogenation. *RSC Adv.* **2014**, *4*, 20948–20954. [[CrossRef](#)]
42. Posada-Pérez, S.; Viñes, F.; Rodriguez, J.A.; Illas, F. Fundamentals of methanol synthesis on metal carbide based catalysts: Activation of  $CO_2$  and  $H_2$ . *Top. Catal.* **2015**, *58*, 159–173. [[CrossRef](#)]
43. Rodriguez, J.A.; Liu, P.; Stacchiola, D.J.; Senanayake, S.D.; White, M.G.; Chen, J.G. Hydrogenation of  $CO_2$  to methanol: Importance of metal-oxide and metal-carbide interfaces in the activation of  $CO_2$ . *ACS Catal.* **2015**, *5*, 6696–6706. [[CrossRef](#)]



© 2016 by the authors; licensee MDPI, Basel, Switzerland. This article is an open access article distributed under the terms and conditions of the Creative Commons Attribution (CC-BY) license (<http://creativecommons.org/licenses/by/4.0/>).